Process Integration and Optimization for Sustainability (2024) 8:905–918
https://doi.org/10.1007/s41660-024-00400-y

ORIGINAL RESEARCH PAPER

RSM-Based Empirical Modeling and Thermodynamic Analysis of a Solar Flat Plate Collector with Diverse Nanofluids

Ramachandran Thulasiram[1] · S. Murugapoopathi[2] · S. Surendarnath[3] · Beemkumar Nagappan[1] · Yuvarajan Devarajan[4]

Received: 8 September 2023 / Revised: 15 February 2024 / Accepted: 19 February 2024 / Published online: 27 February 2024

Abstract
As the energy demand for household applications is increasing, the utilization of solar energy becomes important in fulfilling the energy needs of electrical and thermal appliances. Harvesting the energy from solar through solar thermal energy systems will be effectively used in household and industrial heating applications where the consumption of electrical energy is predominant. Solar thermal energy is harvested through simple devices like flat plate collectors but involves many challenges. Solar flat plate collectors' thermal efficiency is improved by increasing the heat transfer rate by replacing the regular fluids with nanofluids due to their superior thermo-physical properties. Investigators are driven to find novel energy and exergy analysis by the challenges in effective heat transfer and conservation by improving it by including gold, alumina, and copper oxide nanoparticles. To investigate the energy efficiency characteristics of solar flat plate collectors (FPC), the experiments are carried out by considering the different nanofluids (nanofluids with nanomaterials such as gold (Au) and aluminum oxide (Al_2O_3) as well as copper oxide (CuO) as thermal transport media), flow rates of nanofluids (0.016 kg/s, 0.033 kg/s, and 0.05 kg/s), and with mass fraction of nanoparticles (0%, 0.1%, 0.2%, 0.3%, and 0.4%) in nanofluids as variables, such that the energy efficiency, exergy destruction, second law efficiency, entropy generation, and pressure drop performance indicators. The maximum exergy efficiencies are found with *Au* nanofluids 31.55% and 28.78% at 0.4% mass concentration, which has the enhanced second law efficiency compared to water and other nanofluids. At the same time, exergy destruction is found to be minimum (1183.41 W) for *Au* nanoparticle with 0.4% mass fraction and 0.016 kg/min flow rate. The maximum exergy destruction (1509.95 W) was found in the water with 0% concentration at 0.05 kg/min due to the minimum temperature and base fluid heat flow. The energy efficiency and second law efficiencies are well increased with a slight increase in the pressure drop for the 0.4% mass fraction of Au with Al2O3 and CuO nanoparticles. The DoE-based statistical method, the Box-Behnken method, is employed as an experimental design matrix to develop prediction models for exergy responses and pressure drop characteristics. The models are validated through ANOVA results and verified for the R^2 and R^2_{adj} values (> 0.95), and the results are obtained from the models. The results of prediction models are found to have a good correlation with experimental results, and the maximum error between the prediction results and the experimental results is less than 5%. As a future scope, the models are suggested for optimizing the process variables to improve energy efficiency, exergy destruction, and pressure drop objectives.

Keywords Flat plate collector · Nanofluids · Energy and exergy · Renewable energy · Sustainable practices

Nomenclature

Q_w	Heat gained by water (kW)
m_w	Mass flow rate of water circulated (kg/s)
C_{pw}	Specific heat of water (kJ/kg K)
T_f	Final temperature (K)
T_i	Initial temperature (K)
Q_b	Heat loss from absorber plate (kW)
m_b	Mass of absorber plate (kg)
C_b	Specific heat of absorber plate (kJ/kg K)
Q_L	Energy leak to surroundings (kW)
μ	Viscosity (Pa-Sec)
U_t	Total overall heat transfer coefficient (W/m^2 K)
$T_{m,st}$	Mean temperature (K)
T_a	Ambient temperature (K)
ŋ	Collector efficiency (%)
m_{nf}	Mass flow rate of nanofluid (kg/s)
C_{nf}	Specific heat of nanofluid (kJ/kg K)
I_T	Irradiation per unit area (m^2)

Extended author information available on the last page of the article

A_p	Absorber plate area (m^2)
$\dot{E}_{in}$	Input exergy (kW)
$\dot{E}_s$	Exergy absorbed (kW)
$\dot{E}_{out}$	Exergy at the outlet of the system (kW)
$\dot{E}_l$	Exergy leakage (kW)
$\dot{E}_d$	Destructed exergy (kW)
α	Absorptivity
ΔP	Drop in pressure (kPa)
ρ	Density (kg/m^3)
T_s	Source temperature (K)
T_p	Plate temperature (K)
T_{out}	Outlet temperature (K)
$\dot{S}_{gen}$	Entropy generation (kW/K)
$\dot{Q}_s$	Energy gain from the sun (W)
$\dot{Q}_o$	Heat loss to surroundings (W)
η_{ex}	Exergy efficiency (%)
$\dot{m}$	Mass flow rate (kg/s)
τ	Transmissivity

Introduction

Day to day rise in energy demand in power sectors motivates the researcher to focus on various renewable energy systems. Reduction in fossil fuels and increasing usage make the researchers find alternate resources such as solar, wind, and geothermal biomass (Devarajan et al. 2021). Among other renewable energy, solar energy is one of the most promising, and an enormous amount of radiant energy is utilized to meet the daily requirements in a country like India. Solar power is utilized in many forms, like collectors and thermal energy storage, and the developments in flat plate collectors help in utilizing solar heat energy for household applications like water heating, cooking, air conditioning, and power production. The FPC with nanofluids with different concentrations and sizes of nanoparticles with base fluid attracted the researchers to improve heat transfer enhancements (Munuswamy and Devarajan 2023). Molecular or atomic movements of particles normally increase the energy flow, but introducing nanofluids with base fluids provides augmented heat transfer characteristics for suitable applications. The superior improvement in thermal conductivity, better surface area, good stability, and great movement with nanoparticles with base fluid was observed. The nanoparticle collision with base fluid increased the surface area for heat transfer heat capacity and temperature gradient among the suspended particles. The nanoparticle size, nanomaterial, and conductivity are important factors in selecting suitable nanofluid for enhancing thermal characteristics (Ramasamy et al. 2023).

Rathan Kumar et al. (2022) used flat plate collectors to extract energy and utilize it for different purposes, like water distillation plants in remote areas, to improve energy efficiency by around 2.76%. The optimal performance solar collector was mathematically determined by Chamoli 2013. The optimum result was applied to the collector to improve the performance such as outlet temperature, flow rate, heat transfer, and exergy efficiency. The second law efficiency improved at 4% for 0.008 kg/s flow rate with an aperture area of 9 m^2 for an outlet temperature of 360 K as optimum design values. Using mathematical modeling, the non-uniform temperature distribution in FPCs was determined by varying inlet temperature, flow rate, and radiance for analyzing exergy rate and loss. The optimum correlation was obtained by Madhu and Balasubramanian (2018) for experimental data with statistical modeling. The exergy improvement was obtained as 5.95% with exergy loss of 72.96% variation for non-uniform variation in sun and absorber area for 50 °C entry temperature, 0.05 kg/s mass flow with radiance energy of 800 W/m^2. Naveenkumar et al. (2022) designed the double side solar still using aluminum and glass wool to improve the exergy rate, heat transfer, and evaporation rate with base fluid water and 0.1% (volume basis) Cuo, ZnO, and aluminum oxide nanofluids. The energy efficiency of 21.3%, 19.4%, and 17% and exergy efficiency of 50.1%, 36.8%, and 23.8% were improved for the above three nanofluids. The solar FPC with marquise was designed with water and alumina nanofluid (0.1% volume fraction) with varying flow rates from 1 to 5 Lit/min. The exergy and energy efficiencies were determined under varied inlet and outlet temperatures, flow rates, radiation intensity, and atmospheric conditions. The maximum energy and exergy efficiencies of nanofluid mixed with water observed were 28.2% and 34.4% higher than pure water circulation by Arora et al. (2019). Eltaweel and Abdel-Rehim (2019) designed a lower absorbing capability of solar collectors and better transformation of the energy of the based fluid to improve thermosiphon circulation and carbon nanotubes (10–40 nm diameter) with concentrations of 0.01%, 0.05%, and 0.1% (wt.) with distilled water. The maximum efficiency was attained for nanotubes with 0.1% concentration for 1.5 Lit/min. Circulations were 34.1% with a collector size reduction of 34%, and further forced circulation increased efficiency by 6.2%. The exergy efficiency with nanofluid was improved by 38.21% with distilled water. Verma et al. (2016) experimentally investigated the solar collector with MgO nanofluid with water at various concentrations (0.25, 0.5, 0.75, 1.0, 1.25, and 1.5%) with 0.5, 1.0, 1.5, 2.0, and 2.5 Lit/min, respectively. The thermal and second law efficiency obtained for 0.75% concentration, 1.5 Lit/min flow rate as 9.34% higher, 32.93% improvements with irreversibility of 0.0611W/K. The FPC with CuO nanofluid with water was designed and optimized to improve the collector efficiency by varying the tilting angle, nanoparticle size, and heat loss. Sint et al. (2017) observed that enhancing the volume concentration by up to 2% led to a corresponding improvement in collectors' efficiency of up to 5%, in comparison to water. Choudhary et al. (2020) enhanced the thermal properties and stability under varying MgO concentrations (0.04–0.2%) with flow rate (0.5–2.5 Lit/min). The highest collector efficiency improved at 69.1%, and the energy factor increased by 16.7% with 0.2% concentration at 1.5 Lit/min with the U-V spectroscopy stabilization process. Solar FPC thermo-physical properties were analyzed using carbon nanotubes by Said et al. (2016) to improve the particle size, temperature, and loading using sodium dodecyl sulfate as a surfactant. The first and second law efficiency was improved to 95.12% and 26.15%, as water was 42.1% and 8.8%, respectively. The effective utilization of solar energy with nanofluids, thermal coatings, and booster reflectors has improved the first and second law efficiencies using thermal collectors by Murugan et al. (2022). The intensity of radiant energy maximized outlet temperature and thermal performance with flow rate. The chrome and carbon coatings with absorber plates improved thermal efficiency. Notably, the nanoparticle inclusion with base fluid improved the collector's thermal conductivity and efficiency at specified operating conditions. As a future scope, the authors suggested that the impact of the heat conduction route of Au and Cu and other nanomaterials on the improvements in thermal performance and heat transmission rate of solar thermal collectors must be analyzed.

From the literature survey, it has been identified that most of the researchers conducted experimental investigations using various nanomaterials like aluminum oxide (Al_2O_3), copper oxide (CuO), cerium oxide (CeO_2), and carbon nanotubes with different percentages of mass fraction combinations on the base fluids. The performance was reduced over time, the performance of the fluids was reduced, and the impact of nanomaterials destruction was found to be more in detroiting the base fluid heat transfer characteristics. In such cases, Au is found to be one of the good options as nanoparticles to improve the performance of the base fluid. Also, many researchers discussed three performance parameters: energy efficiency, exergy destruction, second law efficiency and pressure drop in the FPC.

The novelty of the work lies in the systematic exploration and optimization of solar flat plate collectors using a combination of nanomaterials, detailed testing, statistical analysis, and the development of accurate prediction models for practical applications. This research extensively analyzes energy efficiency, exergy destruction, second law efficiency, entropy generation, and pressure drop characteristics of solar FPCut with Cu, alumina, and gold nanoparticles-based nanofluids. The nano particle concentrations are varied from 0.1 to 0.5% and with different flow rates of nanofluids (0.016–0.05 kg.s). A hypothesis is developed for objectives as empirical models for the response's energy efficiency, energy destruction, second law efficiency, and pressure drop are developed using the response surface method. The models developed are verified for adequacy and compared with the experimental responses. The detailed discussion on the impact of the variables on the performance parameters was also discussed with future scope.

Fabrication and Testing of Solar Flat Plate Collector with Nanofluids

The solar collector is designed with an occupied area of 2000 mm × 1000 mm × 100 mm with an absorption area of 1.9m^2, as shown in Fig. 1. The absorber plate is a corrugated sheet made of copper of 0.4-mm thickness. The header pipes are made of copper with 25-mm diameter. The riser tubes are made of copper of 12.5-mm diameter and welded under the corrugated design of the absorber plate. The side and collector bottom are covered with glass wool insulation to avoid heat loss. A glass cover of 4-mm thickness made of toughened glass is placed on the top of the collector.

The specifications of the solar collector are provided in Table 1. To test the performance of the collector with nanofluids, the $Al_2O_3 - H_2O$, $CuO - H_2O$, and $Au - H_2O$ nanofluids were prepared with 0.1%, 0.2%, 0.3%, and 0.4% by volume concentration of nanoparticles. In the two-step process, Triton X-100 (surfactant) of 0.02% was mixed with deionized (distilled) water to avoid nanoparticle agglomeration. Followed by blending of Al_2O_3, CuO, and Au nanoparticles in the size range of 20–40 nm with water using the ultrasonicator to get homogeneous suspension. The properties of nanofluids prepared and were calculated using the following relations (Eqs. 1–4) (Ramasamy et al. 2023) and are tabulated (Table 2).

$$\rho_{nf} = \rho_{nf}(\phi) + \rho_{nf}(1 - \phi) \tag{1}$$

$$\mu_{nf} = \frac{\mu_{bf}}{(1 - \phi)^{2.5}} \tag{2}$$

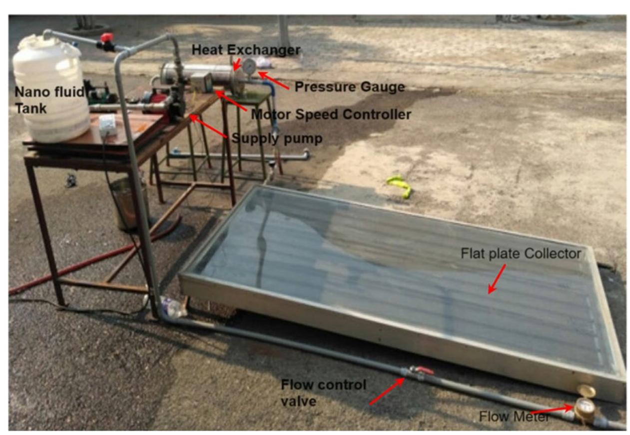

Fig. 1 Solar flat plate collector with nanofluids experimental setup

Table 1 Specifications of the solar flat plate collector

Description	Value
Occupied area	2030 mm × 1000 mm × 100 mm
Absorber area	1.901 m^2
Fluid inlet temperature	25 °C
Convective heat transfer of water	16.4 W/m^2K
Flux on the tilted surface	1069.7 W/ m^2
Conductivity heat transfer coefficient	0.6142
Absorber plate material	Copper
Absorber plate thickness	0.2 mm
Thermal conductivity of absorber plate	350 w/m k
Convective heat transfer coefficient between plate and cover	3.8 w/m^2k
Transmissivity, τ	0.8095
Emissivity, ρ	0.1305–0.1854
Absorptivity, α	0.94
Glass cover material	Toughened glass
Thickness of the glass cover	4 mm
Thermal conductivity, K	0.045 W/mK
Refractive index of glass reactive to air (n)	1.526
Reflectivity	0.076
Cover plate to air spacing,(dcp)	25 mm
Casing	Extruded "Al" section with aluminum sheet on the back side
Riser tube material	Copper
Riser dimensions	13.6 mm OD and 12.5 mm ID
Header pipe material	Copper
Header pipe dimensions	26.4 mm OD and 25 mm ID
Insulation material	Glass wool
Back insulation thickness (glass)	50 mm
Side insulation thickness	25 mm
Conductivity of back insulation, K	0.04 W/m–k
Collector slop, β	11.9°
Wind speed, v	4 m/s
Optical efficiency, η_o	0.82
Emissivity of the absorber plate,ε_p	0.95
Emissivity of the covers,ε_c	0.90
Collector efficiency factor, F'	0.97
Overall heat loss,U_1	5 W/m^2k

$$\frac{k_{nf}}{k_{bf}} = \frac{k_{np} + 2k_{bf} + 2\left(k_{np} - k_{bf}\right)}{k_{np} + 2k_{bf} + \left(k_{np} - k_{bf}\right)\phi} \tag{3}$$

$$C_{p,nf} = C_{p,np}(\phi) + C_{p,bf}(1 - \phi) \tag{4}$$

The variation of viscosity, specific heat, density, and thermal conductivity of Al_2O_3, CuO, and Au nanofluids with different nanoparticle concentrations are shown in Table 2.

Energy and Exergy Analysis of Solar Flat Plate Collector

The maximum work extracted from the system under different operating conditions is energy. The energy analysis describes the effectiveness of each device under preferred operating conditions. The energy analysis determines the amount of energy production during its operation. However, at the same time, energy analysis does not describe the quantity of useful energy available or transformed. For optimum utilization of

Table 2 Properties of nanofluid against nanoparticle concentration

Fluid	Density (kg/m^3)	Viscosity (Pa-sec)	Thermal conductivity (W/mK)	Specific heat (J/kgK)
Water	997.13	0.00089	0.613	4180
Al_2O_3—0.1%	1294.41	0.00111	0.807	3839.5
Al_2O_3—0.2%	1591.7	0.00133	1.046	3499
Al_2O_3—0.3%	1888.9	0.00156	1.350	3158.5
Al_2O_3—0.4%	2186.2	0.00178	1.748	2818
CuO—0.1%	1548.4	0.00111	0.795	3816
CuO—0.2%	2099.7	0.00133	1.019	3452
CuO—0.3%	2650.9	0.00156	1.297	3088
CuO—0.4%	3202.2	0.00178	1.655	2724
Au—0.1%	2829.4	0.00111	0.816	3774.9
Au—0.2%	4661.7	0.00133	1.069	3369.8
Au—0.3%	6493.9	0.00156	1.394	2964.7
Au—0.4%	8326.2	0.00178	1.827	2559.6

energy, in order to reduce entropy generation, exergy analysis is required. The exergy analysis locates the energy degradation of the device quantitatively. The efficiency improvements are associated with various operating conditions named energy and exergy analysis. The exergy efficiency gained major attention from researchers due to its losses associated with different devices. The energy destructed in many forms is called irreversibility caused by friction, pressure drop, mixing, flow rate, radiation, and convective losses in the plate and fluid. The exergy analysis measures the useful energy recoverable from the system and quantifies energy destroyed or entropy generated. The demand for energy, fossil fuel depletion, cost, and thermal system design makes more attention towards energy and exergy analysis to improve optimal energy usage with minimum cost and environmental balance.

Energy Analysis of Solar FPC

Energy and exergy analysis of solar FPC were carried out to discuss the first and second law analysis of thermodynamics in this study. The first law discusses only efficiency of solar collectors but the losses in various devices like absorber plate, storage tank, solar radiation, and leakage of energy from the solar collectors were dealt with exergy analysis using the following relations (Eqs. 5–12).

$$Q_w = m_w C_{pw}(T_f - T_i) \tag{5}$$

$$Q_b = m_b C_b(T_f - T_i) \tag{6}$$

$$Q_L = U_t(T_{m,st} - T_a) \tag{7}$$

$$T_{m,st} = (T_i + T_f)/2 \tag{8}$$

$$A = \pi r^2$$

$$U_l = U_t + U_b + U_s \tag{9}$$

$$U_t = \left[\frac{N}{C\left(\frac{T_p - T_a}{N+f}\right)^{0.33}} + \frac{1}{h_w}\right]^{-1} + \left[\frac{\sigma\left(T_p^2 + T_a^2\right)\left(T_p + T_a\right)}{\left(1/\varepsilon_p\right)\left(\frac{2N+f-1}{\varepsilon_g}\right) - N}\right] \tag{10}$$

$$U_b = \frac{k_i}{t_i} \tag{11}$$

$$U_s = \frac{A_{cs}k_i}{A_p t_i} \tag{12}$$

The thermal efficiency of the flat plate solar collector (η) is the ratio of energy storage in the storage tank to the total solar radiation on the collector, which can be expressed as

$$\eta = m_{nf}C_{nf}(T_f - T_i)/(I_T A_p) \tag{13}$$

Collector efficiency factor (F') is given by the relation

$$F\prime = \frac{1/U_l}{W\left\{\frac{1}{U_l[D+(W-D)F]} - \frac{1}{\pi Dh}\right\}} \tag{14}$$

Exergy Analysis of Solar FPC

Exergy is the maximum output that can be achieved relative to the environment temperature. The general equation of the exergy balance is (Eq. 15)

$$\dot{E}_{in} + \dot{E}_s + \dot{E}_{out} + \dot{E}_l + \dot{E}_d = 0 \tag{15}$$

The inlet exergy rate measures the fluid flow and the absorbed solar radiation rate. The inlet exergy rate with fluid flow can be calculated by Sarhaddi et al. (2010) using the following relation (Eq. 16).

$$\dot{E}_{in,f} = \dot{m}C_p\{T_{in} - T_a - T_a\ln(T_{in}/T_a)\} + (\dot{m}\Delta P_{in}/\rho) \tag{16}$$

where ΔP_{in} is the pressure difference of the fluid with the surroundings at entrance and *r* is the fluid density.

The absorbed solar radiation exergy rate is calculated as:

$$\dot{E}_{in,Q} = \eta I_T A_p(1 - (T_a - T_s) \tag{17}$$

T is apparent sun temperature and equals to 75% of black-body temperature.

Total inlet exergy rate of the solar collector can be calculated as:

$$\dot{E}_{in} = \dot{E}_{in,f} + \dot{E}_{in,Q} \tag{18}$$

At steady state conditions, where the fluid is flowing, the stored exergy rate is zero.

$$\dot{E}_s = 0 \tag{19}$$

When only the exergy rate of outlet fluid flow is considered, the outlet exergy rate can be defined as Devarajan et al., (2021)

$$\dot{E}_{out,f} = -\dot{m}C_p\{T_{out} - T_a - T_a ln(T_{out}/T_a)\} + (\dot{m}\Delta P_{out}/\rho) \tag{20}$$

The heat leakage from the absorber plate to the environment can be defined as the leakage exergy rate and calculated.

$$\dot{E}_l = -UA_p(T_p - T_a)\left[1 - \left(\frac{T_a}{T_p}\right)\right] \tag{21}$$

where the overall heat loss coefficient *U* is optimized at 4.6797 w/m^{2}K (Sarhaddi et al. 2010).

The destroyed exergy rate caused by the temperature difference between the absorber plate surface and the sun can be expressed.

$$\dot{E}_{d,\Delta T_s} = -\eta I_T A_p T_a\left[\frac{1}{T_p} - \frac{1}{T_s}\right] \tag{22}$$

The destroyed exergy rate by pressure drop is expressed by (Suzuki 1988):

$$\dot{E}_{d,\Delta P} = -\frac{\dot{m}\Delta P}{\rho}\{T_a\ln(T_{out}/T_a)/(T_{out} - T_{in})\} \tag{23}$$

The destroyed exergy rate caused by the temperature difference between the absorber plate surface and the agent fluid can be calculated from (Suzuki 1988):

$$\dot{E}_{d,\Delta T_f} = -\dot{m}C_p T_a\left[\ln\left(\frac{T_{out}}{T_{in}}\right) - \frac{T_{out} - T_{in}}{T_p}\right] \tag{24}$$

So, the total destroyed exergy rate can be calculated from:

$$\dot{E}_d = \dot{E}_{d,\Delta T_s} + \dot{E}_{d,\Delta P} + \dot{E}_{d,\Delta T_f} \tag{25}$$

The exergy destruction rate can also be expressed from:

$$\dot{E}_d = T_a\dot{S}_{gen} \tag{26}$$

where *S gen* is the overall rate of entropy generation and can be calculated from (Bejan 1996)

$$\dot{S}_{gen} = \dot{m}C_p\ln(T_{out}/T_{in}) - \dot{Q}_s/T_s + \dot{Q}_o/T_a \tag{27}$$

where Q_S is solar energy absorbed (W) by the collector surface as expressed.

$$\dot{Q}_s = I_T(\tau\alpha)A_p \tag{28}$$

And Q_O is the heat loss to the environment (W),

$$\dot{Q}_o = \dot{Q}_s - \dot{m}C_p(T_{out} - T_{in}) \tag{29}$$

Ultimately, combining all the expression above, the exergy efficiency equation of the solar collector can be analyzed (Sarhaddi et al. 2010):

$$\eta_{ex} = \frac{\dot{m}\left[C_p\left[T_{out} - T_{in} - T_a\ln(T_{out}/T_{in})\right] - \left(\frac{\Delta P}{\rho}\right)\right]}{\left[I_T A_p(1 - \left(\frac{T_a}{T_s}\right)\right]} \tag{30}$$

Empirical Modeling of Energy, Exergy, and Pressure Drop in FPC

To avoid the computational cost of complex engineering problems with high-fidelity simulations and recursive experimental investigations, using empirical models is the surrogate in keeping the engineering designs explorable given the design space. Statistical techniques are highly preferred in developing empirical models for problems where a smaller number of experiments are possible and where the responses are to be generated with no direct dependency on the variables. A set of combinational parameters from the range of variables is plugged into the empirical model to quickly estimate the responses without conducting the complete analysis. Box-Behnken Design (BBD) is a kind of statistical technique used in the response surface methodology (RSM) and is specially designed to fit second order mathematical model. The BBD is an independent and quadratic design that contains fractional factorial design, and the treatment of the model is a combination of midpoints and edges of problem space (Demirpolat et al. 2021). The BBD designs are almost rotatable orthogonal designs made of three, four, and five-level factors that fix the mid-point between the lowest and highest values of the range provided. Including center points in the BBD helps estimate the coefficients for the second-order model by making rotatable designs. Due to this use of face-centered and rotatability of design heredity, the BBD requires a meager number of experimental runs to achieve the empirical model. To generate the BBD and develop the response functions for the problem defined in this article, a standard statistical package, Minitab 17, is used. The Minitab handles a wide set of available data for tasks like data consolidation, analysis, and reporting. Also, from past research, the DoE is more accurate, consistent, and simpler than traditional manual estimation techniques. The set of three-level experimental orthogonal blocks is created using the BBD, for which a second-order full quadratic can be fitted for the response surface model. To investigate the exergy analysis on the solar flat plate collector and to create a hypothesis, the energy efficiency (first law efficiency), exergy destruction, second law efficiency (η_{II}), and pressure drop (ΔP) were considered as responses. The design matrix is generated using BBD for the variables of nanofluids, the mass fraction of the nanoparticles, and the mass flow rate of the nanofluids as per the range shown in Table 3. The design matrix contains 20 experiments generated (Table 4) within the range of variables considered. The experiments are conducted on the solar flat plate collector to determine the energy efficiency, exergy destruction, second law efficiency, and pressure drop for the 20 experiments defined by the BBD. The results of the experiments of BBD are analyzed for the model development and verified for the model adequacy. The significance of the RSM quadratic models developed and tested through ANOVA for the *Fisher* test and *P*-test. The results of ANOVA for the quadratic models energy efficiency, exergy destruction, second law efficiency, and the pressure drop are shown in Table 4.

The development of empirical correlations using the Minitab 17 (DoE) software was carried out through the following steps.

Step 1: Selection and finalization of the design variables and their ranges (Table 3)
Step 2: Selection of the appropriate DoE model from the Minitab 17 software, according to the level of the ranges available. Considering all three variables and their possible range levels, a three-factor, three-level, face-centered, nearly rotatable Box-Behnken design was chosen.
Step 3: Using the chosen design, the experiment uncoded experimental design matrix was generated, containing 20 different sets of experiments.
Step 4: The respective set of experiments is conducted to determine responses that require empirical correlations.
Step 5: Simulate the results of the responses and conduct the ANOVA test, *P*-test, and *F*-test to verify the R^2 and ${R_{adj}}^2$ values to confirm the fitness of the experimental results for the respective responses.
Step 6: Develop the empirical correlations from the respective coefficients table and verify the responses obtained from the correlations for a set of variables within the range defined.

Table 3 The range of variables for the exergy analysis

Parameter	Range	
	Min	Max
Nanoparticle fraction, NF	0	2
Mass fraction, MF (%)	0	0.4
Flow rate, FR (kg/s)	0.016	0.05

The empirical prediction equation is generated based on influencing variables with a 95% confidence level, and the adequacy of the model is tested through ANOVA of each response (Table 4). The *p* value represents the degree of confidence level of coefficients, and the correlations are assessed for the closeness to a 95% probability level. In the ANOVA, *p* values for first-order and second-order parameters of response should be less than 0.05 and are deemed to be relevant. If the *p* value is beyond 0.05, it is considered insignificant on both first and second-order parameters and hence omitted from the approximation function. In this model generated, the parameters for all the responses are found to be significant as the *p* values are found to be less than 0.005.

The ANOVA table findings also provided the testing regression parameters R^2 and ${R_{adj}}^2$ used to test the model suitability and validate the model for prediction efficiency. The R^2 is obtained from the regression variables that minimize the variation in the prediction model. If the value is closer to unique, the model completely complies with the data experimented with and is identified as more precise. The R^2 and R^2_{adj} values of the energy efficiency, exergy destruction, second law efficiency, and pressure drop in the prediction regression models are closer to one. They can forecast the characteristics of the responses for the set of design variables in their defined range. Based on the coefficients obtained from the models, the prediction models (Eqs. 27–30) are developed for the response parameters and used to predict the approximate responses. The experimental results shown in Table 5 and the second-order regression equation representing the energy efficiency, exergy destruction, second law efficiency (η_{II}), and pressure drop (ΔP) are expressed as a function of the parameters of the collector (Eqs. 31–34,). Using the quadratic polynomial model, the relationship between responses and the responses is obtained in actual units. The responses from the prediction model

Table 4 RSM design matrix and the comparison of experimental and predicted results

Run order	Nano-fluid, NF	Mass fraction MF, %	Flow rate, FR (kg/s)	Energy efficiency, η_I (%)			Exergy destruction (W)			Second law efficiency, η_{II} (%)			Pressure drop (ΔP) (N/m^2)		
				Exp	Predicted	Error (%)	Exp	Predicted	Error (%)	Exp	Predicted	Error (%)	Exp	Predicted	Error (%)
1	0	0.2	0.033	58.97	58.9	−0.044	1429.56	1428.06	0.105	19.66	19.99	1.63	5664.9	5910.52	4.16
2	0	0	0.05	57.56	57.8	0.231	1479.96	1478.09	0.126	10.13	10.30	1.64	3721.4	3829.55	2.82
3	2	0.2	0.033	63.96	63.9	−0.018	1373.31	1375.61	−0.167	29.71	29.52	−0.64	16,680.0	17,050.20	2.17
4	2	0.4	0.05	70.93	71.1	0.139	1383.26	1383.28	−0.002	27.92	27.92	0.00	30,987.4	30,925.27	−0.20
5	1	0.2	0.05	69.26	69.2	−0.013	1447.71	1447.38	0.023	16.41	16.29	−0.71	8074.6	7962.45	−1.41
6	0	0.4	0.05	64.44	64.3	−0.148	1432.58	1434.45	−0.130	17.27	17.25	−0.09	8152.3	8508.37	4.18
7	1	0.2	0.033	59.38	59.6	0.225	1419.43	1420.01	−0.041	21.47	21.42	−0.25	7650.5	7575.36	−0.99
8	1	0	0.05	55.99	55.8	−0.176	1509.95	1512.27	−0.153	4.63	4.46	−3.85	285.0	288.00	1.04
9	0	0.4	0.033	55.33	55.4	0.042	1405.67	1405.82	−0.010	23.93	23.76	−0.70	7849.7	7483.70	−4.89
10	2	0	0.016	39.99	40.1	0.130	1404	1402.21	0.128	21.70	21.85	0.71	3328.1	3209.96	−3.68
11	1	0.4	0.016	52.94	53.2	0.224	1271.83	1271.25	0.045	47.84	48.05	0.43	11,944.4	12,331.77	3.14
12	1	0.2	0.05	69.26	69.2	−0.013	1447.71	1447.38	0.023	16.41	16.29	−0.71	8074.6	7962.45	−1.41
13	0	0.4	0.033	55.33	55.4	0.042	1405.67	1405.82	−0.010	23.93	23.76	−0.70	7849.7	7483.70	−4.89
14	1	0.2	0.033	60.01	59.6	−0.399	1419.43	1420.01	−0.041	21.47	21.42	−0.25	7650.5	7575.36	−0.99
15	2	0.4	0.016	60.38	60.1	−0.230	1183.41	1184.63	−0.103	63.63	63.42	−0.34	27,586	27,296.00	−1.06
16	1	0.2	0.033	59.38	59.6	0.225	1419.43	1420.01	−0.041	21.47	21.42	−0.25	7650.5	7575.36	−0.99
17	2	0	0.05	57.56	57.5	−0.056	1509.95	1510.09	−0.010	5.29	5.29	−0.03	3721.4	3990.45	6.74
18	1	0.4	0.033	57.91	57.8	−0.083	1379.8	1376.97	0.205	28.76	29.11	1.18	14,375	14,712.53	2.29
19	2	0.2	0.05	72.67	72.7	0.028	1426.32	1424.42	0.133	20.80	21.04	1.16	17,681.8	17,511.90	−0.97
20	0	0	0.016	37	36.9	−0.129	1454.8	1455.96	−0.079	13.61	13.46	−1.12	3328.1	3347.51	0.58

Table 5 Model adequacy for fitting of second-order model

Model	Energy efficiency	Exergy destruction	Second law efficiency	Pressure drop
p value	< 0.0001	< 0.00001	< 0.00001	< 0.00001
SD	0.59	74.21	0.131	7926.4
Mean	0.59	1410.2	0.23	10,113
R^2	99.95	99.96	99.98	99.9
Adj. R^2	99.93	99.93	99.97	99.81

results show that the responses obtained from the regression model agree with experimental responses (Table 4), and the error between the results falls within 5%.

$$\begin{aligned} \text{Energy efficiency} = {} & 0.31689 - 0.01186I * NF + 1.2409 * MF \\ & + 2.307 * FR + 0.01824\, NF * NF - 2.1027 \\ & * MF * MF + 58.25 * FR * FR + 0.08829NF \\ & * MF - 0.5211 * NF * FR - 4.744 * MF * FR \end{aligned} \tag{31}$$

$$\begin{aligned} \text{Exergy destruction} = {} & 1369.10 - 9.60 * NF - 670.1 * MF \\ & + 6980 * FR - 18.21 * NF * NF + 560.4 \\ & * MF * MF - 96056 * FR * FR - 105.07 \\ & * NF * MF + 1243.9\, NF * FR + 6763 \\ & * MF * FR \end{aligned} \tag{32}$$

$$\begin{aligned} \text{Second Law efficiency } \eta_{II} = {} & 0.27510 + 0.00680\, NF + 1.3138 \\ & * MF - 11.297 * FR + 0.03336 * NF * NF \\ & - 1.1093 * MF * MF + 157.09 * FR * FR \\ & + 0.19592 * NF * MF - 1.9712 * NF * FR \\ & - 13.924 * MF * FR \end{aligned} \tag{33}$$

$$\begin{aligned} \text{Pressure drop } \Delta P = {} & 1168 - 7713\, NF + 345 * MF + 173531 \\ & * FR + 3794 * NF * NF + 1967 * MF * MF \\ & - 2338560 * FR * FR + 27846 * NF * MF \\ & + 4117 * NF * FR + 201477 * MF * FR \end{aligned} \tag{34}$$

Results and Discussions

Effect of Mass Fraction on Thermal Conductivity

The first and second law efficiencies mainly depend on the conductivity of nanofluids. Figure 2 shows the variation in mass fraction of different nanofluids with thermal conductivity. The conductivity of nanofluids increases with an increase in mass fractions. The suspended nanoparticles tend to increase the conductivity of the base fluid with an increase in mass fractions. The thermal conductivity of nanofluids variation of Au is higher than CuO and Al_2O_3 due to diameter, porosity, nanomaterial, and mass fraction (Said et al 2016). The temperature variation with solar radiation improves the thermal conductivity of various nanofluids due to molecular dispersion and density variation (Murugan et al. 2022).

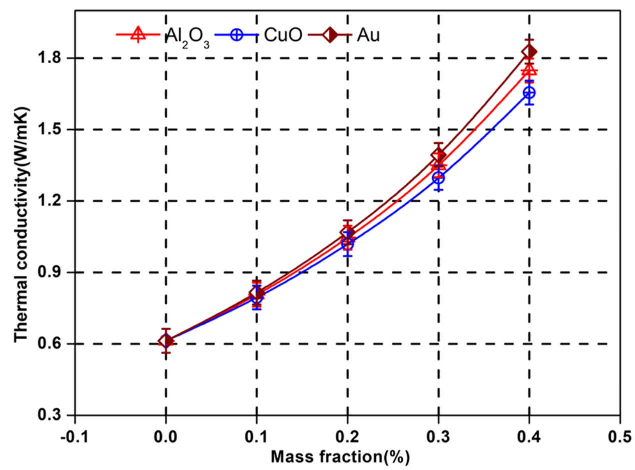

Fig. 2 Variation in thermal conductivity with mass fraction

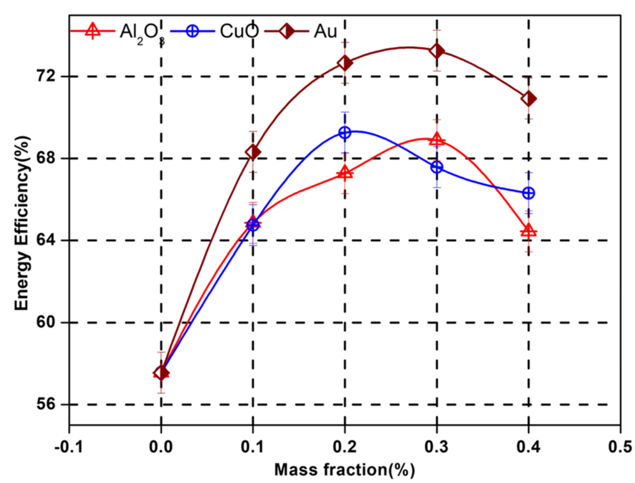

Fig. 3 Variation in energy efficiency with mass fraction

Effect of Mass Fraction on Energy Efficiency

The mass fraction of different nanofluids with energy efficiency is given in Fig. 3. The energy efficiency is one factor in identifying the losses in energy in different forms. The energy efficiency improved with temperature and mass fraction of nanofluid concentration. However, the improved mass concentration increased fluid viscosity prominently to intensify the frictional losses. The variation in solar energy radiation varies with the volume fraction of various nanoparticles that could improve the efficiency of collectors. By experiment, the maximum energy efficiency for FPC is found to be 6.34% and 8.41% higher for 0.3% Au mass fraction based Al_2O_3 and CuO nanofluids. Further improvements in mass fraction increased the viscosity of various nanofluids, which decreased the energy efficiency. At the same time, the energy efficiencies obtained from the empirical correlations for 0.3% Au mass fraction are found to be 6.29% and 8.481% for the Al_2O_3 and CuO nanofluids. This shows the closeness of the results of the prediction model.

Effect of Mass Fraction on Pressure Drop

The pressure variation with a combination of nanofluid concentration for various mass fractions is given in Fig. 4. The increase in mass concentration increases the viscosity of the nanofluids, which gives resistance to the fluid movements. The flow resistance increases the pumping power, but at the same time, it improves the heat transfer rates of different nanofluids. The Au nanoparticle pressure drop was higher than other nanofluids with different mass concentrations. There was an improvement in heat transfer with pressure drop due to increased nanoparticle concentration, density, and decrease in velocity (Bayareh 2022).

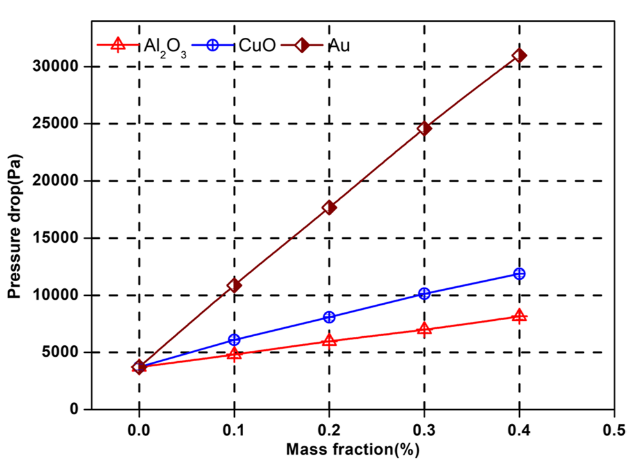

Fig. 4 Variation in pressure drop with mass fraction

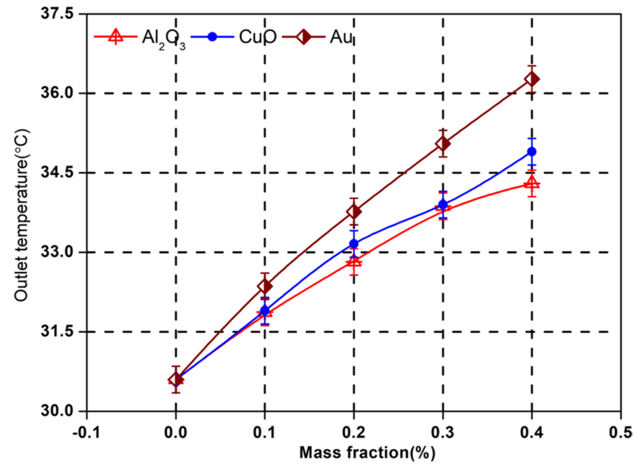

Fig. 5 Variation in outlet temperature with mass fraction

Effect of Mass Fraction on Outlet Temperature

Figure 5 shows the outlet temperature of different nanofluids with mass concentrations of Au, CuO, and Al_2O_3. The outlet temperature is the one key parameter that directly affects solar collectors' energy efficiency under varying operating conditions. The variation in nanoparticle concentration with water improves the outlet temperature of the fluids in solar collectors. The Au nanoparticle maximum outlet temperature was 3.92% and 5.74% higher than 0.4% mass concentration CuO and Al_2O_3.

Effect of the Mass Fraction on Exergy Efficiency

The second law efficiency of various nanofluid concentrations with different nanoparticles is shown in Fig. 6. The exergy efficiency mainly depends on the mass

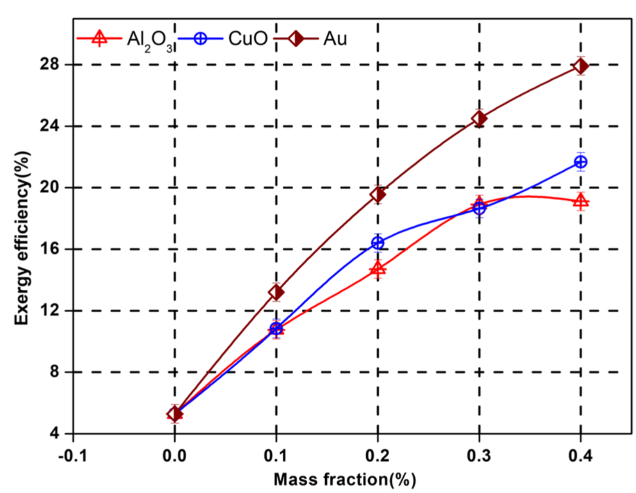

Fig. 6 Variation in exergy efficiency with mass fraction

concentration, size, and nanoparticle material. The *Au* nanoparticle performance was higher than other nanofluids, and an increase in mass concentration improved the collector efficiency due to the maximum heat flow rate. The maximum exergy efficiency of *Au* was 31.55% and 28.78% higher than Al_2O_3 and *CuO* at 0.4% mass concentration. The enhanced second-law efficiency of Au nanoparticles in solar collectors may improve the collectors' performance compared to water and other nanofluids (Kumar et al. 2020).

Effect of the Mass Fraction on Entropy Generation

The entropy generation is the reverse of the exergy efficiency of solar collectors, and the cause of irreversibility is due to the friction and pressure losses associated with the entropy generation of various nanoparticles. The nanoparticle mass fraction of *Au*, *CuO*, and Al_2O_3 with entropy generation is presented in Fig. 7. The Au nanoparticle mass concentration varies from 0 to 0.4%, decreasing the entropy generation by 9.15% due to improved heat transfer and outlet temperature variation. For *CuO* and Al_2O_3 nanoparticle, the entropy generation decreases by 6.45% and 5.39% for the same operating conditions. The increased thermal conductivity and improved heat flow greatly decreased the entropy generation in solar collectors. At lower mass concentrations, the entropy generation increased due to the time the base fluid and absorber plate took to conduct heat (Bejan 1996).

Effect of the Mass Fraction on Exergy Destruction

The exergy destruction of various nanofluids with mass concentrations is shown in Fig. 8. The exergy destruction decreases with an increase in mass concentration due to the particle's nanoparticle size, nanomaterial, and heat capacity.

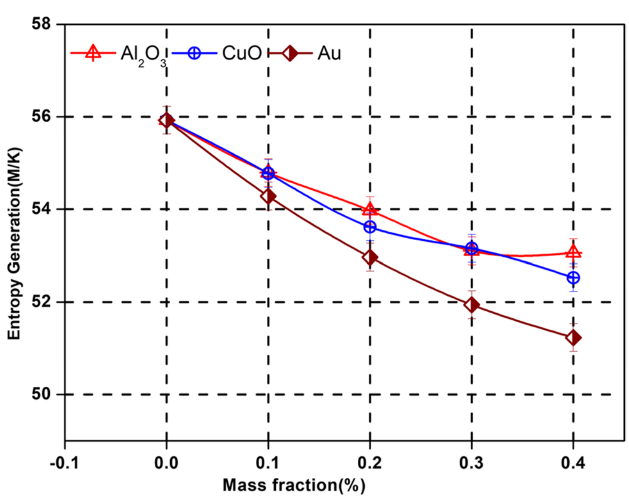

Fig. 7 Variation in entropy generation with mass fraction

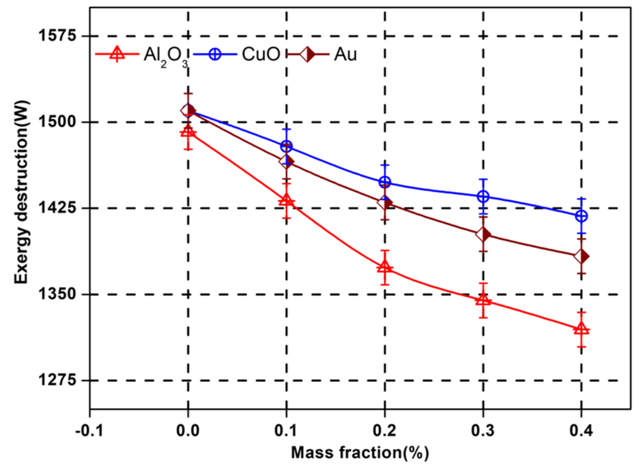

Fig. 8 Variation in exergy destruction with mass fraction

The minimum destruction found for 0.4% mass fraction of *Au*, *CuO*, and Al_2O_3 was 1323.86 W, 1418.2 W, and 1319.38 W, respectively, due to improved outlet temperature and enhanced heat flux in the absorber plate due to nanoparticle concentration. The maximum exergy destruction was found for water at 0% concentration as 1509.95 W due to more heat required for heating water without nanoparticle concentration. Exergy destruction decreases with increased mass fraction of various nanoparticles due to density variation, collector intensity, and fluid friction caused concentration and viscosity of various nanofluids (Dharmalingam et al. 2017).

Effect of System Variables on Responses

The effect of the variables on the responses particular regions of interest on responses is analyzed through response surfaces. Figure 9 shows the variation in the surface plot of pressure drop, mass flow rate, and mass fraction for the averaged mass concentration of various

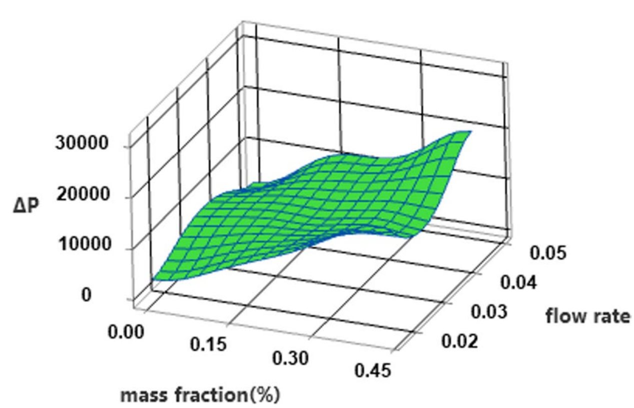

Fig. 9 Surface plot of pressure drop against the flow rate and mass fraction %

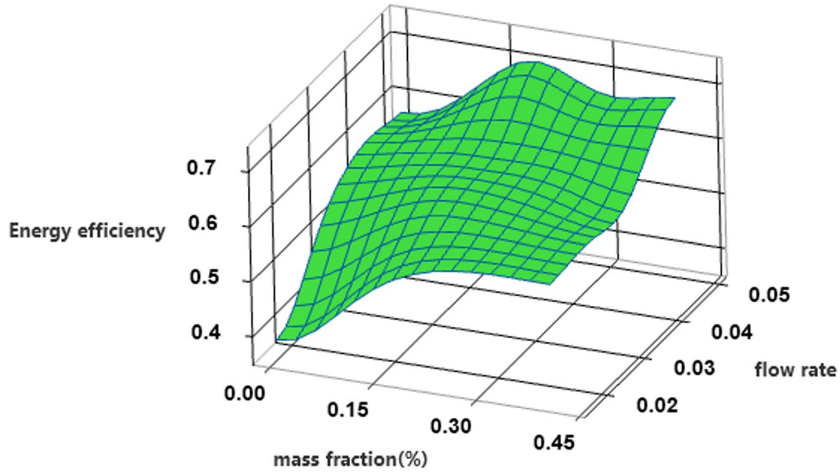

Fig. 10 Surface plot of energy efficiency against the flow rate and mass fraction %

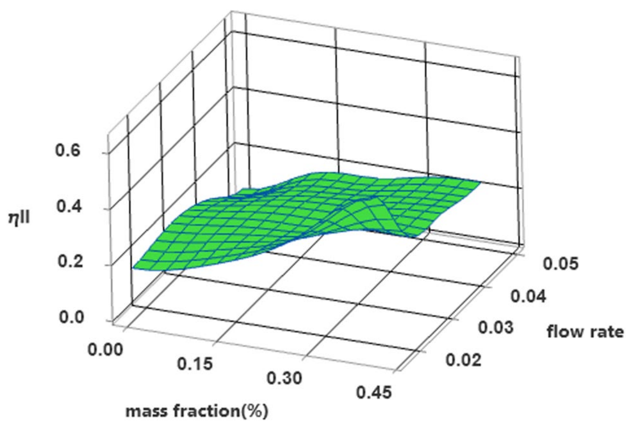

Fig. 11 Surface plot of second law efficiency (η_{II}) against the flow rate and mass fraction %

nanoparticles. Pressure drop increases with mass concentration and particle size increase and optimum at 0.03 kg/min flow rate. Figure 10 shows the surface plot of energy efficiency with flow rate and mass fraction for the averaged mass concentration of different nanoparticles. The collectors' efficiency improved with nanoparticle concentration and flow rate (Seralathan et al. 2023). The optimum efficiency was obtained for Au nanofluid with 0.2% concentration and 0.05 kg/s. The outlet temperature and heat flow improved with nanoparticle mass concentration and flow rate. The second law of efficiency depends on solar collectors' flow rate, particle concentration, and outlet temperature (Singh and Yadav 2022). Figure 11 shows the second law efficiency with flow rate and mass fraction of *Au*, *CuO*, and Al_2O_3 nanofluids. The maximum exergy efficiency was 63.63% for Au nanofluid with 0.016 kg/s at 0.4% mass fraction. The *Au* nanoparticle shows superior behavior to other nanoparticles due to its thermal conductivity and specific heat capacity (Khosravi et al. 2022). Figure 12 shows the surface plot of exergy destruction with flow rate and mass fraction of different nanoparticles. Exergy destruction decreases with increasing nanoparticle concentration and mass flow rate of nanofluid (Mahdavi et al. 2022). The minimum exergy destruction observed was 1183.41 W for *Au* nanoparticle with 0.4% mass fraction and at 0.016 kg/

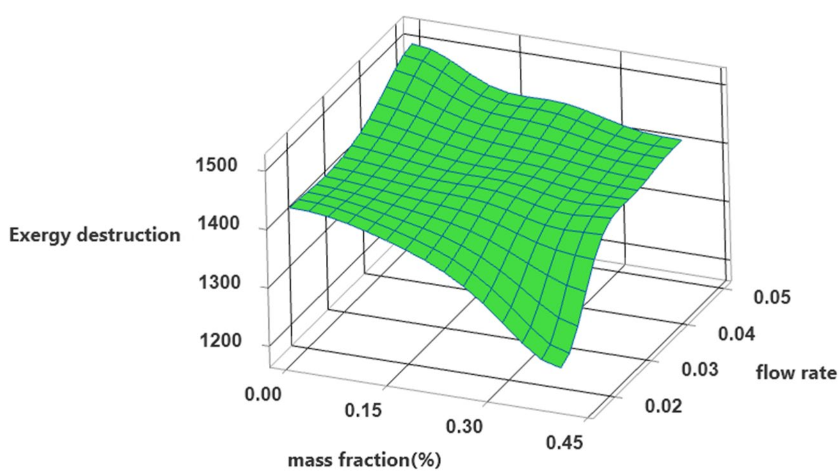

Fig. 12 Surface plot of energy destruction against the flow rate and mass fraction %

min flow rate. The maximum exergy destruction of 1509.95 W was found for water at 0% concentration at a flow rate of 0.05 kg/min due to lower temperature and base fluid heat flow than the nanoparticle (Dharmalingam et al. 2017).

Conclusion

The study conducted a comprehensive analysis of energy and exergy on flat plate collectors using water-based Au, CuO, and Al_2O_3 nanofluids with varying mass fractions and flow rates. The empirical correlations developed for energy efficiency, exergy destruction, second law efficiency, and pressure drop using a response surface methodology (RSM) approach were found to predict the responses for the defined variables with an error of less than 5%. The study identified that the addition of nanoparticles, particularly 0.4% mass fraction of Au with Al_2O_3 and CuO, showed improved second law efficiencies of 31.55% and 28.78%, respectively. It was observed that the pressure drop increased with the addition of nanoparticles, with a higher pressure drop in nanofluids with Au nanoparticles. The energy efficiency of the collector improved significantly with a maximum of 0.2% nanoparticle concentration, particularly with Au nanoparticles at 0.2% mass fraction, showing the maximum energy of 72.96% compared to other combinations. Furthermore, the study inferred that the use of nanoparticles in flat plate collectors improved heat transfer and energy efficiency with minimum entropy generation by increasing flow rates. The Au-based nanofluids with 0.2% mass fraction and at a mass flow rate showed comparatively better heat transfer rate and entropy generation.

The findings of this study are significant as they provide valuable insights into the impact of nanofluids on the performance of flat plate collectors. The results demonstrate the potential for significant improvements in energy efficiency and heat transfer rates by utilizing nanofluids, particularly with specific mass fractions and flow rates. These findings are consistent with previous research that has highlighted the improved thermal efficiency of flat plate solar collectors when conventional heat transfer fluids are replaced with nanofluids. The study's emphasis on the reduction of entropy generation and the enhancement of energy efficiency aligns with the broader goal of optimizing the parameter for maximizing energy efficiency and second law efficiency while minimizing exergy destruction and pressure drop in solar collector systems. This research contributes to the understanding of the thermal performance enhancement of flat plate solar collectors using nanofluids, particularly in terms of energy efficiency, exergy destruction, and second law efficiency. The findings underscore the potential for significant improvements in heat transfer and energy efficiency by leveraging nanofluids, thereby offering valuable insights for the optimization of solar collector systems in the future.

Author Contribution Murugapoopathi S and Ramachandran T conceived the idea of the work.

Beemkumar Nagappan and Yuvarajan Devarajan designed the experiments.

Surendarnath S supervised the study.

Data Availability The datasets used and/or analyzed during the current study are available from the corresponding author upon reasonable request.

Code Availability Not applicable.

Declarations

Ethics Approval and Consent to Participate Not applicable.

Consent for Publication Not applicable.

Competing Interests The authors declare no competing interests.

References

Arora S, Fekadu G, Subudhi S (2019) Energy and exergy analysis of marquise shaped channel flat plate solar collector using Al2O3–water nanofluid and water. J Solar Energ Engg 141(4). https://doi.org/10.1115/1.4042454

Bayareh M (2022) Exergy analysis of solar chimney power plants: a review. Sustain Energy Technol Assess 53:102568. https://doi.org/10.1016/j.seta.2022.102568

Bejan A (1996) Entropy generation minimization: the new thermodynamics of finite-size devices and finite-time processes. J Appl Phys 79(3):1191–1218. https://doi.org/10.1063/1.362674

Chamoli S (2013) Exergy analysis of a flat plate solar collector. J Energ South Africa 24(3):8–13. https://doi.org/10.17159/2413-3051/2013/v24i3a3137

Choudhary S, Sachdeva A, Kumar P (2020) Investigation of the stability of MgO nanofluid and its effect on the thermal performance of flat plate solar collector. Renew Energy 147:1801–1814. https://doi.org/10.1016/j.renene.2019.09.126

Demirpolat AB, Aydoğmuş E, Arslanoğlu H (2021) Drying behavior for Ocimum basilicum Lamiaceae with the new system: exergy analysis and RSM modeling. Bio Conver Biorefine 12(2):515–526. https://doi.org/10.1007/s13399-021-02010-x

Devarajan Y, Nagappan B, Choubey G, Vellaiyan S, Mehar K (2021) Renewable pathway and twin fueling approach on ignition analysis of a dual-fuelled compression ignition engine. Energ & Fuels 35:9930–9936. https://doi.org/10.1021/acs.energyfuels.0c04237

Devarajan Y, Nalla BT, Babu MD, Subbiah G, Mishra R, Vellaiyan S (2021) Analysis on improving the conversion rate and waste reduction on bioconversion of Citrullus lanatus seed oil and its characterization. Sustain Chem Pharm 1;22:100497

Dharmalingam R, Kandasamy R, Sivagnana Prabhu KK (2017) Lorentz forces and nanoparticle shape on water based Cu, Al 2 O 3 and SWCNTs. J Mol Liq 231:663–672. https://doi.org/10.1016/j.molliq.2016.11.048

Eltaweel M, Abdel-Rehim AA (2019) Energy and exergy analysis of a thermosiphon and forced-circulation flat-plate solar collector using MWCNT/water nanofluid. Case Stud Therm 14:100416. https://doi.org/10.1016/j.csite.2019.100416

Khosravi K, Mohammed HI, Mahdi JM, Silakhori M, Talebizadeh Sardari P (2022) Developing a predictive model and multi-objective optimization of a photovoltaic/thermal system based on energy and

exergy analysis using response surface methodology. SSRN Electro J. https://doi.org/10.2139/ssrn.4171638
Kumar A, Sharma M, Thakur P, Thakur VK, Rahatekar SS, Kumar R (2020) A review on exergy analysis of solar parabolic collectors. Sol Energy 197:411–432. https://doi.org/10.1016/j.solener.2020.01.025
Madhu S, Balasubramanian M (2018) Effect of swirling abrasives induced by a novel threaded nozzle in machining of CFRP composites. Int J Adv Manuf Technol 95:4175–4189. https://doi.org/10.1007/s00170-017-1488-2
Mahdavi N, Mojaver P, Khalilarya S (2022) Multi-objective optimization of power, CO2 emission and exergy efficiency of a novel solar-assisted CCHP system using RSM and TOPSIS coupled method. Renew Energy 185:506–524. https://doi.org/10.1016/j.renene.2021.12.078
Munuswamy DB, Devarajan Y (2023) Critical examination of the role of silica nanoparticle dispersions in heat transfer fluid for solar applications. Silicon 15:571–581. https://doi.org/10.1007/s12633-022-02015-9
Murugan M, Saravanan A, Elumalai PV, Kumar P, Ahamed Saleel C, Samuel OD, Setiyo M, Enweremadu CC, Afzal A (2022) An overview on energy and exergy analysis of solar thermal collectors with passive performance enhancers. Alex Eng 61(10):8123–8147. https://doi.org/10.1016/j.aej.2022.01.052
Naveenkumar R, Shanmugam S, Veerappan A (2022) Performance and exergy analysis of solar-operated vacuum fan and external condenser integrated double-slope solar still using various nanofluids. Envi Sci Pollut Res 30(5):12883–12902. https://doi.org/10.1007/s11356-022-22919-8
Ramasamy D, R R, T R, S M, S S (2023) Optimisation of flow and fluid properties of nanofluids to enhance the performance of solar flat plate collector using MCDM technique. Proc Inst Mech Eng C 095440892211507. https://doi.org/10.1177/09544089221150738
Rathan Kumar L, Madhu S, Mothilal T, et al (2022) Effect of walnut powder reinforcement on the mechanical properties of biodegradable natural flax/hemp fibre-based composites. Materials Today: Proceedings 69:1387–1393. https://doi.org/10.1016/j.matpr.2022.09.203
Said Z, Saidur R, Sabiha MA, Hepbasli A, Rahim NA (2016) Energy and exergy efficiency of a flat plate solar collector using pH treated Al2O3 nanofluid. J Clean Prod 112:3915–3926. https://doi.org/10.1016/j.jclepro.2015.07.115
Sarhaddi F, Farahat S, Ajam H, Behzadmehr A (2010) Exergetic performance assessment of a solar photovoltaic thermal (PV/T) air collector. Energy Build 42(11):2184–2199. https://doi.org/10.1016/j.enbuild.2010.07.011
Seralathan S, Chenna Reddy G, Sathish S, Muthuram A, Dhanraj JA, Lakshmaiya N, Velmurugan K, Sirisamphanwong C, Ngoenmeesri R, Sirisamphanwong C (2023) Performance and exergy analysis of an inclined solar still with baffle arrangements. Heliyon 9(4):e14807. https://doi.org/10.1016/j.heliyon.2023.e14807
Singh V, Yadav VS (2022) Optimizing the performance of solar panel cooling apparatus by application of response surface methodology. Proc Inst Mech Eng C 236(22):11094–11120. https://doi.org/10.1177/09544062221101828
Sint NKC, Choudhury IA, Masjuki HH, Aoyama H (2017) Theoretical analysis to determine the efficiency of a CuO-water nanofluid based-flat plate solar collector for domestic solar water heating system in Myanmar. Sol Energ 155:608–619. https://doi.org/10.1016/j.solener.2017.06.055
Suzuki A (1988) General theory of exergy-balance analysis and application to solar collectors. Energy 13(2):153–160. https://doi.org/10.1016/0360-5442(88)90040-0
Verma SK, Tiwari AK, Chauhan DS (2016) Performance augmentation in flat plate solar collector using MgO/water nanofluid. Energy Convers Manag 124:607–617. https://doi.org/10.1016/j.enconman.2016.07.007

Authors and Affiliations

Ramachandran Thulasiram[1] · S. Murugapoopathi[2] · S. Surendarnath[3] · Beemkumar Nagappan[1] · Yuvarajan Devarajan[4]

✉ Yuvarajan Devarajan
yuvarajand.sse@saveetha.com

[1] Department of Mechanical Engineering, Faculty of Engineering and Technology, Jain (Deemed-to-Be University), Bangalore, India

[2] Department of Mechanical Engineering, PSNA College of Engineering and Technology, Dindigul, India

[3] Department of Mechanical Engineering, DVR & Dr HS MIC College of Technology (A), Vijayawada, India

[4] Department of Mechanical Engineering, Saveetha School of Engineering, SIMATS, Saveetha University, Chennai, Tamil Nadu, India